Geochemical features of Site 840 from the Tonga Platform. A comparison with the other sites from Leg 135 ODP

Tonga Platform
Leg 135 ODP
Volcaniclastic inputs
Interstitial waters
Diagenesis

Plate-forme Tonga
Leg 135 ODP
Apports volcanoclastiques
Eaux interstitielles
Diagenèse

Frédéric VITALI, Gérard BLANC, Philippe LARQUE and Jean SAMUEL

Centre de Géochimie de la Surface, CNRS UPR n°6251, Institut de Géologie, 1, rue Blessig, 67084 Strasbourg Cedex, France.

Received 3/01/94, in revised form 30/06/94, accepted 12/07/94.

ABSTRACT

The sedimentary sequence recovered at Site 840 ODP in the Tonga Platform is 597 m thick and ranges in age from Holocene to late Miocene. Here, from the 49 samples analysed, three classes of sediments can be identified, based on their proportion of biogenic carbonate and volcanogenic content. These three classes are comparable with those previously differentiated in the Lau Basin (Sites 834-839) and with some sediments from the Tonga Trench Margin (Site 841). In constrast with neighbouring Site 834-839 sediments from the Lau Basin, the Site 840 sediment composition appears to be exempt of hydrothermal ponding material and seems to be characterized only by biogenic and terrigenous andesitic-rhyolitic volcanic inputs. The alteration of volcanic material results principally in the replacement of the volcanic glass by smectite. This alteration is the major cause of the observed changes in the Ca, Mg, and K gradients in the interstitial waters. Diagenetic processes seem to be more pronounced in the deeper part of the hole, with the formation of abundant zeolite minerals.

RÉSUMÉ

Caractéristiques géochimiques du Site 840 de la Plate-forme Tonga. Comparaison avec les autres sites du Leg 135 ODP.

597 m de sédiments d'âge Holocène à Miocène supérieur ont été traversés et carottés lors du forage 840 ODP sur la plate-forme Tonga. À partir des 49 échantillons analysés, trois catégories de sédiments ont été identifiées en fonction de leur pourcentage de carbonate biogénique et de matériel volcanogénique. Ces trois catégories de sédiments sont comparables à celles précédemment décrites dans le Bassin de Lau (Sites 834-839) et à une partie des sédiments du Site 841 de la marge active de la fosse Tonga. À la différence des sédiments des Sites 834-839 localisés à l'ouest de l'arc volcanique actif de Tofua, ceux du Site 840 ne paraissent pas avoir reçu d'apports hydrothermaux. Carbonates biogéniques et turbidites de sédiments de compositions andésitiques à rhyolitiques provenant des volcans proches constituent les deux sources majeures d'apports identifiées. L'altération du matériel volcanique entraîne essentiellement la formation de smectite et provoque des variations notables des gradients de concentrations de Ca, Mg et K des eaux interstitielles. La diagenèse précoce semble être plus poussée dans la partie profonde du forage, comme l'atteste la présence de zéolites.

Oceanologica Acta, 1994. **17**, 5, 517-533.

INTRODUCTION

During Leg 135 ODP (December 1990 - February 1991), the R.V. *Joides Resolution* drilled 597 m of sediments at Site 840 on the south central platform, which forms the crest of the active volcanic arc of the Tonga Ridge (Fig. 1). The Tonga Ridge has been in existence in some form since at least the Eocene, when it was a component of an ancestral Melanesian proto-arc comprising the Fiji, Lau, Tonga, and New Hebrides arcs. The structure probably came into existence after the initiation of a subduction zone at some time during the early Eocene. During the late Miocene, approximately 10-12 Ma, the New Hebrides Arc probably separated from the Lau-Tonga-Fiji segment following the inititation of subduction beneath the westerly-facing New Hebrides Trench. The formation of the Lau back-arc basin to the west of the Tonga Ridge from the late Miocene onwards, and the initiation of the currently active Tofua Arc to the north of the Tonga Ridge, have further contributed to the uplift/subsidence history and regional tectonic development of the Tonga Ridge (Parson, Hawkins, Allan *et al.*, 1992).

Site 840, constituted by adjacent holes 840B and 840C, is situated at 22°13.2'S, 175°44.92'W in 754.4 m of water and is located on the west flank of the platform, which at this latitude is about 60 km wide at the 1000 m isobath. The sedimentary sequence drilled at Site 840 is 597.3 m thick and ranges in age from Holocene to late Miocene (Parson, Hawkins, Allan *et al.*, 1992). Core recovery was low, averaging 41%. Consequently, biostratigraphical and

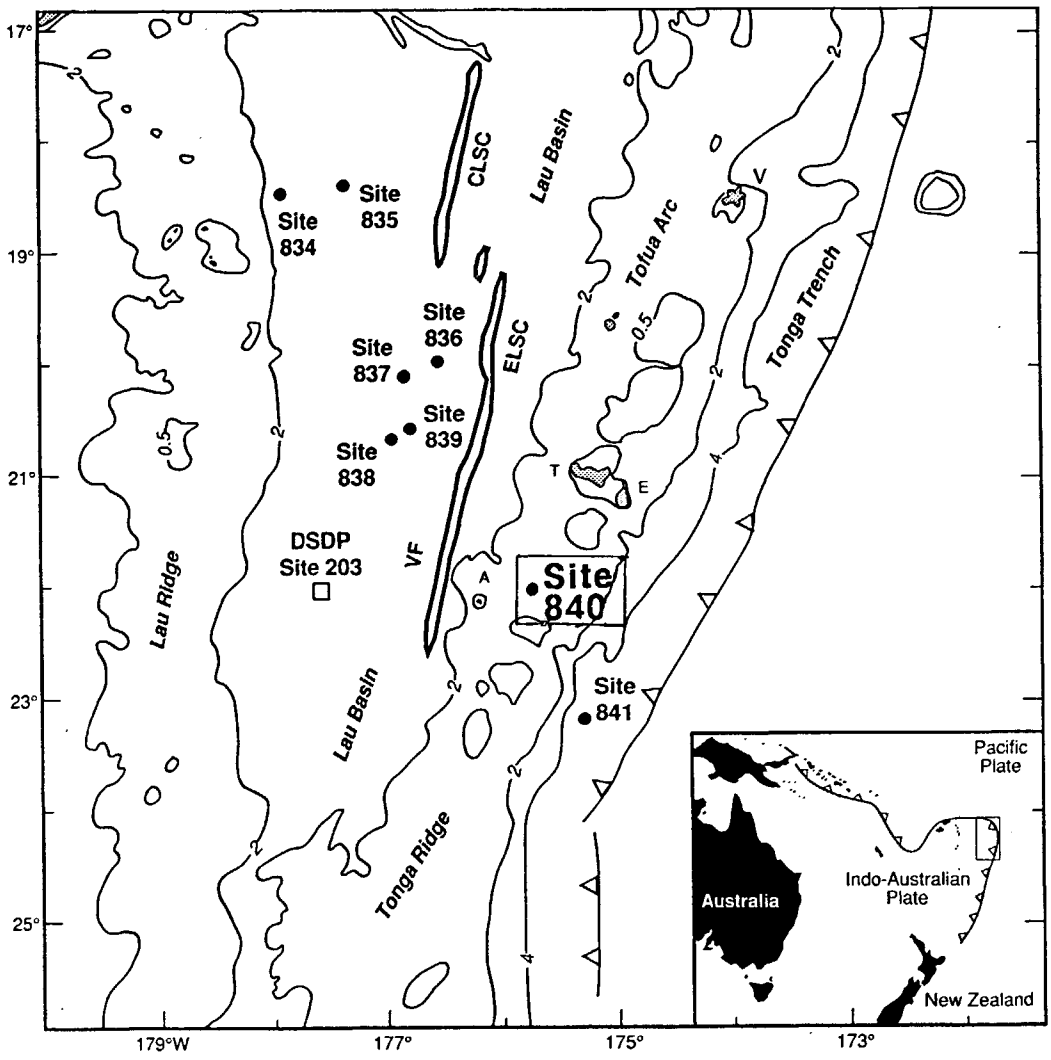

Figure 1

Regional setting of Site 840, with location of other drill sites of the Leg 135 cruise and the major geological features of the Tonga Trench and Lau Basin system (from Parson, Hawkins, Allan et al., *1992).*
Islands include T = Tongatapu Island, E ='Eua Island, V = Vavau Island and A = Ata Island.
CLSC = Central Lau Spreading Centre; ELSC = Eastern Lau Spreading Centre; VF = Valu Fa Ridge.

Localisation du Site 840 de la plate-forme Tonga, et des autres sites forés lors du Leg 135 (834-839, 841), et caractéristiques géologiques majeures de la fosse Tonga et du bassin de Lau (d'après Parson, Hawkins, Allan *et al.*, 1992).
abréviations utilisées: T = île deTongatapu , E = île 'Eua, V = île Vavau, and A = île Ata.
CLSC = Centre d'expansion du bassin de Lau médian ; ELSC = Centre d'expansion du bassin de Lau oriental ; VF = ride de Valu Fa.

lithological resolution is limited within some intervals. However, on the basis of the available data, a schematic lithostratigraphic log was drawn up (Fig. 2). The sequence is subdivided into three sedimentary units. Unit I comprises the sediments from the sea floor down to 109.98 m below sea floor (mbsf) and consists of nannofossil oozes, vitric silts, vitric sands, and pumiceous gravels. Unit II extends from 109.98 mbsf to 260.5 mbsf and is dominated by nannofossil chalks and pumiceous gravels, although vitric siltstones and vitric sandstones are also common. Unit III extends from 260.5 to 597.3 mbsf and comprises a sequence of volcaniclastic turbidites of vitric sandstone and siltstone interbedded with nannofossil chalk. Near the base of the sequence, there are also beds of volcaniclastic breccia and conglomerate. Upward through the unit, the refining and thinning of individual turbidites occur, indicating a change from proximal to more distal deposition. Sedimentation rates ranged from 110 to 820 mm/k.y. during the late Miocene but diminished with the decrease in volcanic activity during the Pliocene, and dropped to 14 mm/k.y. through the Pleistocene (Parson, Hawkins, Allan *et al.*, 1992).

In the present paper, the sediments of Site 840 will be characterized mineralogically and chemically, in order to evaluate the temporal and compositional variation of arc volcanism and to characterize the factors responsible for the chemical variations of interstitial water, which reflect the intensity of the diagenetic processes. The chemical and mineralogical composition of sediments from Site 840 from the Tonga Platform will be compared with that of sediments cored during the same Leg in the nearby Lau Basin and in the Tonga Trench Margin. This comparison will allows us to characterize the chemical and mineralogical variation from a back-arc basin to an active margin and to determine the major parameters which influenced the sedimentation, such as biodetritic, volcanic and hydrothermal inputs.

In the Lau Basin, hydrothermal activity was previously detected by mineralogical and chemical analyses of numerous surface sediment samples from this SW Pacific area (Cronan *et al.*, 1984, 1986; Moorby *et al.*, 1986; Hodkinson *et al.*, 1986) and established during later submersible cruises (von Stackelberg *et al.*, 1985; 1988; 1990, Fouquet *et al.*, 1990, 1991). Calculations of high accumulation rates of the hydrothermal fraction in the Lau Basin sediments strongly suggest hydrothermal activity over a period of 4 m.y. in the back-arc basin (Blanc, 1994). In this study, we shall determine whether this hydrothermal activity, in the form of hydrothermal precipitates carried in the water column, has an influence on the Tonga Platform and Tonga Margin sediment composition. We shall also define the change in the nature of the volcanic products from the back-arc Lau Basin to the active Tonga Margin.

EXPERIMENTAL METHODS

Sediment analysis

The variation of mineralogy with depth will be established on the basis of the mineral percentages estimated on 49 samples of Site 840, from the peak intensity using mass absorption coefficients and chemical data (Hooton and Giorgetta, 1977).

Mineralogy

The mineralogical composition of the major mineral phases was determined on dry powdered sediments by X-Ray Diffraction (XRD) techniques using a Phillips PW 1710. The samples were run between 3° and 65° 2 θ at 40KV/20 mÅ, using CuKα radiation, and a scan speed of 1°/min. For some samples, the clay fraction (< 2 μm) was separated and X-ray diffraction analyses were done on the following four types of oriented aggregates: untreated, ethylene-glycol treated, hydrazine treated, and heated (4 hours at 490 °C).

Element analysis

All bulk sediment samples were powdered in a carbon steel mill, dried at 110 °C for 12 hours, and then ashed at 1000 °C for 3 hours. Loss-on-ignition (L.O.I.) measurements resulted from the weight difference between dried and calcined samples. Sample splits of 100 mg were fused for 20 minutes with 750 mg of pure lithium tetraborate under inert Ar atmosphere in a crucible (Carbone Lorraine V25), and were dissolved as a molten fusion product in a glycerin-hydrochloric acid solvent. The addition of glycerin increases the solubility of borate acid and stabilizes the solution viscosity, consequently increasing the reproducibilities of the flux injection and of the intensity of the spectrum lines (Samuel *et al.*, 1985). The 1:250 final dilution was then introduced into the spectrometers. Concentrations of Na and K were determined on a Corning Flam emission spectrometer, and Si, Al, Mg, Ca, Fe, and Ti were determined on an ARL 14000 arc spectrometer. Mn, Sr, Ba, P, V, Cr, Ni, Co, Zn, Cu, Zr, Y, La, Ce, Yb and Lu were analysed using an ARL 35000 ICP-AES (Inductively Coupled Plasma - Atomic Emission Spectrometer). The accuracy of the analyses was determined by comparison with international marine sediment standards previously analysed at the CRPG, the ANRT, and the USGS. These standards are as follows: SD01 (East Pacific Rise Sediment), SD02 (Central Pacific Sediment) and MAC3 (Marine Mud). The accuracy of our analyses was within 5% for all determined elements. The precision of the analyses, as determined from duplication of the sample preparation, was between 2 and 5% for the major elements. The precision was generally 5% for the minor elements at concentrations 10 times the detection limit and 20% for those at 5 times the detection limit, which gives a general precision of 5% for Mn, Sr, P, Ba, V, Cr, Zn, Cu, Sc, Y, Zr, La, Ce and Yb and 20% for Ni, Co, and Lu. The contents of the major elements are expressed in oxide weight per 100 g dried sample (Wt.%, Table 1) and the contents of the minor and rare earth elements are given in ppm (Tables 2 and 3).

Interstitial water analysis

The method of obtaining interstitial water from the sediment using a stainless steel press was described in detail by Manheim and Sayles (1974). Interstitial water was collected in 50 cm^3 syringes and filtered through a 0.45-μm Mil-

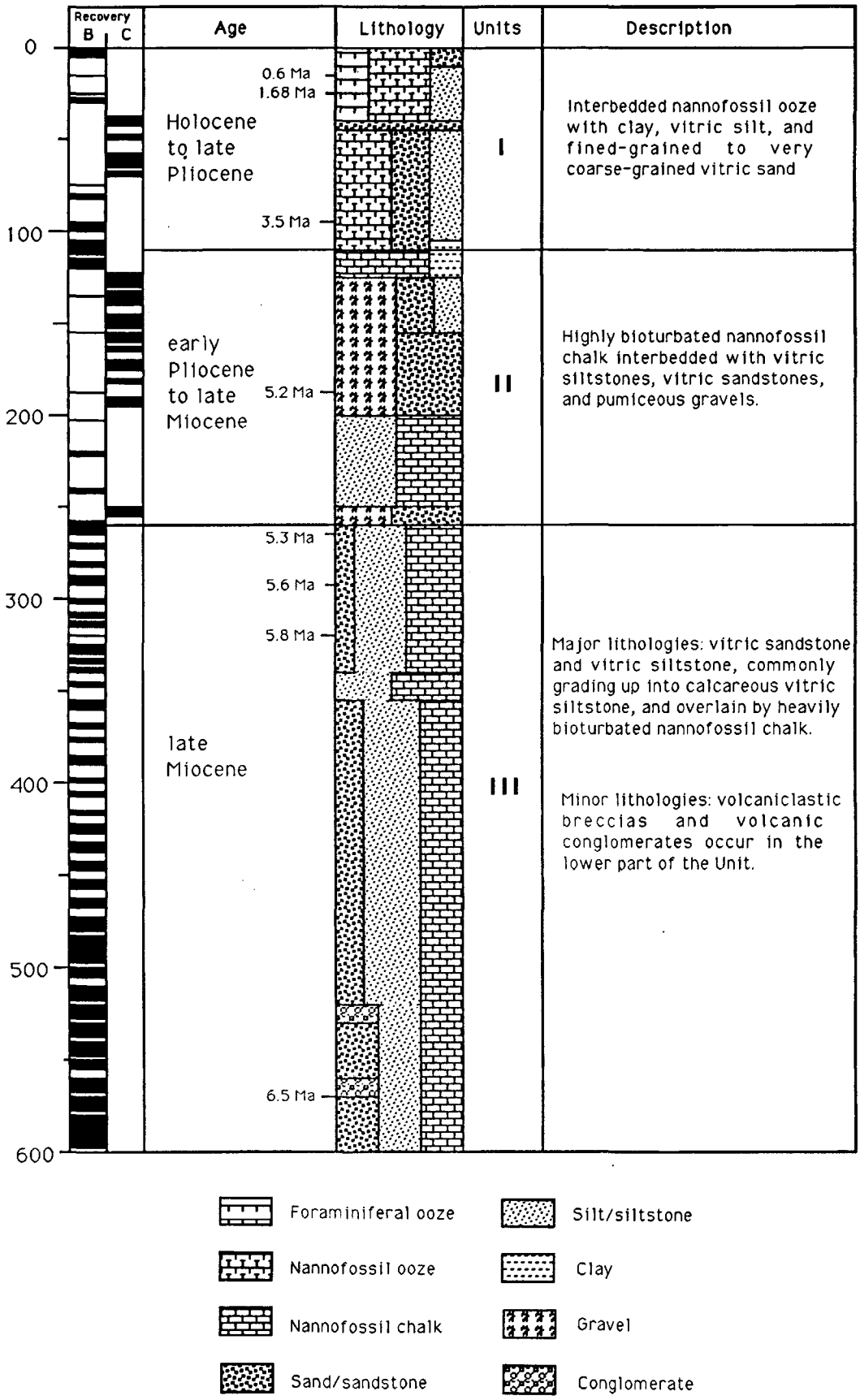

Figure 2

Summary of lithologic units for Site 840.

Unités lithologiques du Site 840.

nºODP	Hole	Depth (mbsf)	Lost 1000ºC (Wt %)	SiO2 (Wt %)	Al2O3 (Wt %)	MgO (Wt %)	CaO (Wt %)	Fe2O3 (Wt %)	Na2O (Wt %)	K2O (Wt %)	TiO2 (Wt %)	Total (Wt %)
4XCC	B	28.46	16.55	46	8.7	1.7	18.4	4.9	2.72	0.36	0.55	99.88
1H2	C	41.14	23.31	33.3	7.5	1.53	27.6	4.5	1.56	0.2	0.42	99.92
3H2S	C	59.9	5.36	58.2	13.5	3.15	7.3	8.1	3.27	0.7	0.59	100.17
4H4S	C	72.5	24.06	33.8	7.2	1.18	28	3.6	1.28	0.26	0.34	99.72
10X1	B	86.2	40.13	8.6	1.7	0.46	46.8	1	0.07	0.05	0.1	98.91
11X2	B	96.21	37.57	13.8	2.8	0.58	42.5	1.3	0.07	0.05	0.13	98.8
12X4	B	111.5	39.44	9.1	2.5	0.83	44.9	2.1	0.06	0.05	0.18	99.16
13X2	B	118.1	37.13	12.4	3	0.9	42.4	2.5	0.05	0.05	0.2	98.63
5H1	C	125.5	23.43	33.8	7.9	0.94	26.9	3.2	1.84	0.48	0.41	98.9
15CC	B	134.42	29.75	27.1	5.5	0.73	31.7	2.3	1.02	0.3	0.32	98.72
6H3	C	136.77	5.47	58.6	14	1.85	5.2	6.4	4.82	0.95	0.8	98.09
7H2	C	146	13.02	51.5	10.9	1.02	15.1	3.7	3.47	0.84	0.56	100.11
8H3	C	155.86	6.57	62.5	12.9	1.3	4	4.3	5.42	1.33	0.61	98.93
12H2	C	193.31	7.44	62.7	12.7	1.12	3.5	5.1	5.51	1.4	0.64	100.11
24X1A	B	221.49	39.25	8.3	2.5	0.5	46.8	1	0.07	0.05	0.11	98.58
26X1	B	240.79	24.04	35.3	7.2	1.38	25.8	3.6	1.75	0.43	0.35	99.85
13H4	C	255.48	3.53	58.5	14	3.09	6.6	9.6	4.04	0.63	0.82	100.81
28X2	B	262.21	26.24	28	7.4	2.44	27.8	4.9	1.25	0.1	0.41	98.54
29X1	B	269.99	21.87	32.4	8.8	3.12	24.6	6.5	1.48	0.18	0.55	99.5
33X1	B	308.64	5.16	54.3	14	5.26	4.6	10.8	4.17	1.22	0.9	100.41
34X1	B	318.45	13.78	40.3	12.6	4.12	19.2	7.8	1.99	0.22	0.62	100.63
35X2	B	330.02	4.78	55.5	13.7	3.6	6.4	9.5	4.24	0.93	0.96	99.61
36X1	B	333.37	7.3	58.5	13.1	2.72	6	7	3.49	1.02	0.7	99.83
37X1	B	338.22	6.13	59	13	2.61	4.9	7.3	3.53	0.9	0.63	98
39X2	B	359.01	6.52	63.5	12.1	2.81	2.5	5.4	3.66	1.78	0.29	98.56
40X1	B	367	25.78	27	7.2	2.08	30.2	4.2	1.13	0.16	0.38	98.13
41X1	B	376.41	28.08	23.6	6.2	1.72	35.4	3.8	0.72	0.12	0.33	99.97
42X1	B	387.04	15.52	40.6	10.6	2.35	19.3	6.3	2.26	0.49	0.5	97.92
43X1	B	395.85	7.62	48.9	14.5	4.69	9.6	9.9	3.44	0.85	0.86	100.36
44X1	B	405.36	10.96	55.2	11	3.24	8.1	5.9	3.3	1.09	0.42	99.21
45X2	B	416.36	24.22	31.7	7.5	2.26	26.2	5	1.68	0.83	0.44	99.83
46X1	B	424.72	13.76	43.3	10.4	5.4	12.8	9.1	2.91	1.1	0.84	99.61
47XCC	B	435.25	5.48	57.4	13.5	3.64	5.3	9.5	3.38	0.91	1.01	100.12
48X3	B	446.37	16	40.2	11	3.8	19.5	7	2.03	0.33	0.56	100.42
49X1	B	452.61	10.79	44.6	12.8	4.64	12.4	9	2.57	0.51	1.01	98.32
50X1	B	463.06	6.85	59.9	13.4	2.95	4.4	7.8	3.09	0.91	0.78	100.08
51X1	B	472.18	15.7	41.6	11	3.66	18.3	6.5	2.09	0.39	0.62	99.86
52X5	B	487.7	20.4	35.3	9.9	3.15	23.2	5.5	1.76	0.26	0.59	100.06
53X4	B	496.58	8.3	63.1	12.3	2.21	3.1	5.7	3.13	1.54	0.64	100.02
54X1	B	500.98	19.21	37.7	9.6	2.26	21.5	4.9	2.06	0.44	0.47	98.14
55X3	B	514.3	15.2	44.5	10.1	3.15	16.6	6.7	2.36	0.66	0.57	99.84
56X4	B	525.15	4.57	55.9	13.5	3.87	6.1	10.7	3.23	0.52	0.94	99.33
57X2	B	532.36	21.87	33.6	8.4	3.23	25.2	5.8	1.51	0.2	0.51	100.32
58X5	B	546.22	8.05	65.1	11.8	1.23	2.6	4.8	3.79	1.79	0.39	99.55
59X3	B	552.08	6.96	54	13.4	4.2	4.5	10.1	4.28	1.32	0.89	99.65
60X1	B	560.08	6.24	53.3	13.2	5.12	4.6	11.3	3.96	1.24	0.91	99.87
61X2	B	570.13	6.45	54	13.8	4.49	3.7	11.2	4.32	1.2	0.94	100.1
62X6	B	586.55	7.96	60.3	13.1	3.57	3	6.4	3.64	0.96	0.73	99.66
63X3	B	592.11	16.75	41.9	10.5	3.03	18	5.6	2.24	0.46	0.64	99.12

Table 1

Major element composition of bulk sediment, Site 840.

Composition des éléments majeurs du sédiment total, Site 840.

n°ODP	Hole	Depth (mbsf)	Mn (ppm)	P (ppm)	Sr (ppm)	Ba (ppm)	V (ppm)	Ni (ppm)	Co (ppm)	Cr (ppm)	Zn (ppm)	Cu (ppm)	Sc (ppm)	Y (ppm)	Zr (ppm)
4XCC	B	28.46	1569	872.8	658	122	63.9	30.7	20.9	39.8	61.2	13.1	18.9	24.9	43.8
1H2	C	41.14	1565	785.5	809	115	96.4	29.7	21.8	3.7	56.6	15	15.2	21.1	34.7
3H2S	C	59.9	973	741.8	200	154	157	27.3	33.5	15.4	72.5	63.9	27.9	25.9	60.7
4H4S	C	72.5	1044	916.4	857	126	59.4	33.9	15	1	49.2	12.9	12.3	18.5	32.5
10X1	B	86.2	646	741.8	1328	50.9	14.7	33	5	3.3	12.9	6.7	3	12.4	9.4
11X2	B	96.21	594	741.8	1235	79.6	25.1	28.1	10.1	5.6	18.7	19.1	4.5	15.6	34
12X4	B	111.5	586	872.8	1283	55.9	48.1	37.6	24.3	12.3	19.4	12.7	5.9	10	12.1
13X2	B	118.1	867	872.8	1465	70.9	56.9	37.1	12.5	8.3	23.4	18.6	6.2	10.6	19.4
5H1	C	125.5	1546	1047.3	793	155	31.8	38.7	10.1	1.6	57.2	10.8	8.9	23.2	66.9
15CC	B	134.42	2040	829.1	1033	134	23.6	28	9.7	5.6	36.4	5.8	6.6	18.9	54.7
6H3	C	136.77	1336	1091	239	170	70.7	24.4	10.4	1	79.5	19.6	17	32.7	100
7H2	C	146	1620	916.4	492	215	32.7	30.8	8.6	1	67.3	11.2	12.5	30.4	96
8H3	C	155.86	998	960	205	224	44.6	24.9	13.5	1.4	168	15.9	14.2	35.3	118
12H2	C	193.31	1012	960	170	219	33	30.7	5	2.3	60.3	19.4	13.8	38.8	136
24X1A	B	221.49	2058	741.8	1144	43.4	25.7	34.5	13.3	5.8	14.9	14.4	4.5	12.2	14.3
26X1	B	240.79	1728	916.4	684	114	40.1	38.5	10.7	21.9	65.2	15.3	11.8	22.9	48.1
13H4	C	255.48	1205	785.5	158	119	234	36.8	16.4	5.9	81	62.4	28.3	26.8	67
28X2	B	262.21	1524	916.4	941	93.9	105	34.8	17.7	7.4	72.1	18.7	14.3	17.5	43.3
29X1	B	269.99	1545	916.4	760	92.9	179	39.3	18.5	10.1	71.5	23.8	21	14.5	30.3
33X1	B	308.64	1108	1047.3	154	80.7	189	62.7	24.9	18.1	86.3	76.4	30.2	22.7	76.9
34X1	B	318.45	1487	1003.7	550	86.8	211	47.4	17.7	19.4	75.2	30.7	28.9	18.9	39.4
35X2	B	330.02	1358	1091	207	105	208	49.9	29.3	11.3	86.1	60.3	29.9	29.8	79.1
36X1	B	333.37	1368	916.4	208	134	95.1	19.5	14.1	11.6	103	39.6	32.1	33.1	104
37X1	B	338.22	1232	872.8	189	110	103	16	16.3	13.8	116	55.6	25	32.7	86
39X2	B	359.01	712	567.3	132	145	54.3	7.9	7.9	5.6	68.8	15.5	14	25.4	84.9
40X1	B	367	2702	829.1	908	78.8	118	23.8	13.4	8.3	58.1	22	14.6	16.1	37.7
41X1	B	376.41	3790	872.8	1007	144	79.4	24.9	10.1	11.2	31.5	18.2	12.6	20.4	35.9
42X1	B	387.04	2379	1047.3	549	151	127	18.4	16.3	9.8	70.6	33.1	20.7	25.4	59
43X1	B	395.85	1210	1134.6	297	68.2	280	20.6	28.6	14.5	111	79.2	33.2	28.9	61.9
44X1	B	405.36	1409	872.8	254	135	33.4	13.2	8.8	6.1	77.7	22.2	17	43.7	99.8
45X2	B	416.36	1731	1178.2	1007	334	95.2	32.8	14.1	9.9	62.2	21.7	14.7	31.5	49.1
46X1	B	424.72	1399	960	509	152	244	27.9	19.2	12.7	80.3	90	25.8	21.8	58.7
47XCC	B	435.25	1296	1614.6	212	157	136	14.1	16.3	1	151	81.2	25.2	34.6	102
48X3	B	446.37	1622	1047.3	556	162	140	22	22.4	11	127	71.3	20.4	35.5	64.9
49X1	B	452.61	1175	1265.5	430	125	272	23	26.4	6.8	131	132	31.6	37.1	66.4
50X1	B	463.06	1052	872.8	168	122	115	14.4	14.5	1	143	71.9	23.3	31.3	86.4
51X1	B	472.18	1815	916.4	509	93.1	128	17	15.4	8.4	116	69.1	20.7	23.1	65.3
52X5	B	487.7	2159	960	604	79.6	153	22	16	7.2	94.4	61.7	22.2	23	42.6
53X4	B	496.58	1054	872.8	165	172	40.8	10.5	9.6	1.9	116	63.1	17.1	36	143
54X1	B	500.98	2359	785.5	595	121	109	14.4	11.6	11.1	31.7	38.9	15.6	25.7	50
55X3	B	514.3	1943	916.4	455	167	126	20.2	13	5.2	119	76.2	18.8	30.6	84.5
56X4	B	525.15	1328	916.4	161	73.4	227	19.4	24.9	4.1	166	154	32.9	30.7	75.6
57X2	B	532.36	1966	1047.3	638	65.9	114	24.3	17.7	8.2	94	44.1	17.2	26.5	57.6
58X5	B	546.22	960	741.8	136	198	14.2	8.2	8.6	1.4	102	35.8	14	38.8	158
59X3	B	552.08	1104	872.8	504	55.8	211	14.9	18.8	9.5	155	107	32.2	26	59.4
60X1	B	560.08	1063	916.4	501	48.7	260	16.7	27.4	10.1	164	128	36.5	25.9	60.3
61X2	B	570.13	963	916.4	621	59.8	268	17.8	25.1	10.1	148	125	36.1	29.2	65.5
62X6	B	586.55	1049	1003.7	143	167	51.2	9.5	11.9	3.6	216	106	20.1	37.9	139
63X3	B	592.11	4401	960	466	160	168	21.9	19	14.7	122	75.1	24	25.6	62

Table 2

Minor and trace element composition of bulk sediment, site 840.

Composition des éléments mineurs et traces du sédiment total, Site 840.

nºODP	Hole	Depth (mbsf)	La (ppm)	Ce (ppm)	Yb (ppm)	Lu (ppm)
4XCC	B	28.46	11.6	14.4	2.3	0.1
1H2	C	41.14	2.5	10.4	1.4	0.2
3H2S	C	59.9	2.5	10	2.6	0.2
4H4S	C	72.5	6.3	13.8	1.4	0.7
10X1	B	86.2	13	30.4	0.8	0.2
11X2	B	96.21	14.8	31.5	1	0.3
12X4	B	111.5	13	31.9	0.8	0.3
13X2	B	118.1	9.6	10	0.9	0.3
5H1	C	125.5	2.5	29.2	2.2	0.8
15CC	B	134.42	10.5	20.7	1.7	0.5
6H3	C	136.77	8	25.1	3.5	0.8
7H2	C	146	13.2	19.6	3.4	1.1
8H3	C	155.86	9.7	30.3	3.9	1.1
12H2	C	193.31	13.8	33.3	4.1	0.8
24X1A	B	221.49	15.9	14.5	0.9	0.4
26X1	B	240.79	15.5	10	2.3	0.6
13H4	C	255.48	8	16.4	3.1	1.1
28X2	B	262.21	16.9	16.2	1.6	0.5
29X1	B	269.99	7.9	10	1.1	0.3
33X1	B	308.64	16.5	17.8	2.3	0.6
34X1	B	318.45	8.6	16.8	1.8	0.6
35X2	B	330.02	17.9	37	3.3	1
36X1	B	333.37	20.7	31.8	3.5	0.9
37X1	B	338.22	13.9	33.6	4.4	1.2
39X2	B	359.01	3	25.6	2.7	0.7
40X1	B	367	9.5	20.9	1.7	0.6
41X1	B	376.41	5.9	20.3	1.9	0.7
42X1	B	387.04	10.4	11.4	2.7	0.6
43X1	B	395.85	6.7	10	2.9	0.6
44X1	B	405.36	8.5	16.8	4.5	0.8
45X2	B	416.36	9.6	12.6	2.8	0.5
46X1	B	424.72	8.6	10	1.8	0.3
47XCC	B	435.25	7.9	10	3.6	0.2
48X3	B	446.37	7.1	10	3.8	0.8
49X1	B	452.61	6.5	22.5	3.8	0.5
50X1	B	463.06	6.1	10	3.6	0.5
51X1	B	472.18	9.8	10	2.6	0.7
52X5	B	487.7	10.4	10	2.6	0.7
53X4	B	496.58	12.9	10	4.4	0.9
54X1	B	500.98	*	*	*	*
55X3	B	514.3	12.5	16.6	3.4	0.8
56X4	B	525.15	10.3	10.2	3.6	0.8
57X2	B	532.36	19.5	10	3.1	1.1
58X5	B	546.22	5.9	10	4.7	1.1
59X3	B	552.08	8.2	10	3.3	0.6
60X1	B	560.08	10.6	10	3.1	0.9
61X2	B	570.13	9.5	10	3.7	0.9
62X6	B	586.55	16.2	16.4	4.7	1.2
63X3	B	592.11	9.2	10	2.6	1.2

Table 3

Concentration of La, Ce, Yb and Lu, Site 840.

Concentration de La, Ce, Yb et Lu, Site 840.

lipore filter. International Association for the Physical Sciences of the Ocean (IAPSO) standard sea water P99 was the primary standard for the water analysis aboard ship.

Individual inorganic species were analysed on board (Parson, Hawkins, Allan *et al.*, 1992) according to the procedure outlined by Gieskes and Petersman (1986). Results are expressed in millimoles or micromoles per litre of solution. Sodium concentrations were determined by charge balance. The difference between calculated salinity using Na data and measured salinity did not exceed 3%.

Alkalinity and pH were determined using a Metrohm autotitrator with a Brinkmann combination pH electrode. Alkalinity reproducibility is better than 5%; data are given in millimoles of acid equivalent per litre. Salinity was determined using a Goldberg optical hand refractometer measuring the total dissolved solids. Chloride was measured by silver nitrate titration of a 0.1-ml sample diluted in 5 ml of deionized water using potassium chromate as an indicator. Reproducibility of the IAPSO standard is better than +/– 1%. Sulphate was quantified using a Dionex 2120 ion chromatograph. Reproducibility on different dilutions of the IAPSO standard is better than +/– 2%.

Calcium was determined by complexometric titration of a 0.5-cm^3 sample with EGTA (ethylene-bis-(oxyethylenenitrilo)-tetra-acetic acid) using GHA (2-2'-ethane-diylidine-dinitrilo-diphenol) as an indicator. To enhance the determination of the end point, the calcium-GHA complex was extracted on to a layer of butanol (Gieskes, 1973). Magnesium was determined by EDTA (di-sodium ethylenediamine-tetra-acetate) titration for total alkaline earths (Gieskes, 1973). Subsequent subtraction of the calcium and strontium values yielded the magnesium concentration in the interstitial water sample. Ammonia and silica determinations were carried out using the colorimetric methods described by Gieskes and Petersman (1986).

Atomic absorption measurements were done with a Varian SpectrAA-20 spectrophotometer to determine K, Sr and Mn, all measurements being carried out in absorption mode using an oxidizing air-acetylene flame. Potassium was determined on 1:500 sample dilutions with 1000-ppm cesium chloride as an ionization suppressor. The standard calibration curve used ranged from 0.25 to 1.50 ppm, with a correlation coefficient r = 0.9996. Reproducibility is about +/– 3%. Strontium was determined on 1:20 sample dilutions. Lanthanum trichloride (5000 ppm) was used as a buffer in the sample solution and in the standards. The standard calibration curve ranges from 1 to 5 ppm. The correlation coefficient obtained is r = 0.9998 and reproducibility is better than +/– 2%.

Manganese was determined on 1:5 dilutions of the samples. A 1000-ppm cesium chloride solution was used as an ionization suppressor in the sample solution and in the standards. The standard calibration curve ranges from 0.25 to 3 ppm with a correlation coefficient r = 0.9995. The detection limit of this method is about 10 µM in the sample and the reproducibility is better than 2% for Mn concentrations higher than 20 µM.

RESULTS AND DISCUSSION

Mineralogy and chemistry

Mineral paragenesis

The distribution of the mineralogical content of the sedimentary column (Fig. 3), is calculated from the X-ray peak intensity and chemical data (Table 1) and shows that calcite, clays and amorphous silica are the three dominant phases. Biogenous silica content is negligible, and amorphous silica corresponds predominantly to volcanic glass. With the exception of the three samples from 552.36 to 570.13 mbsf, which are rich in zeolites (32% of the whole rocks on average, with analcime, clinoptilolite, erionite, heulandite as zeolite minerals), the cumulative percent of the three dominant phases ranges between 65% and 95%. In Unit I and the top of Unit II (0-135 mbsf), calcite is the main component of the bulk sediment, associated with clays and amorphous silica. The non-carbonate fraction of

the sediment in this interval averages 45%. Below 135 mbsf, the percentage of the non-carbonate fractions reaches 75% in average, and the sediments are composed mostly of amorphous silica and clays.

Clay mineral analyses were carried out on 26 samples (Table 4). Interlayered illite/smectite constitutes the most important clay assemblage (between 75% and 100%) of the clay paragenesis, with the exception of the 387.04-424.72 mbsf and 525.15-570.13 mbsf zones. In these two parts of the section, the main clay mineral is smectite (more than 90% of the clay fraction). Chlorite is also detected and appears through the entire sequence but in amounts never exceeding 15% of the clay paragenesis.

Plagioclase accounts for 5 to 20% of the entire rock, and quartz content is less than 10%. Below 350 mbsf, the occurrence of small amounts (5% on average) of minerals such as hematite and pyrite is frequent. The calculated amount of halite is an artefact of the sample preparation. Hence, on Figure 3, the weight percentage distribution of the other minerals with depth was normalized to 100% after substraction of the halite amount.

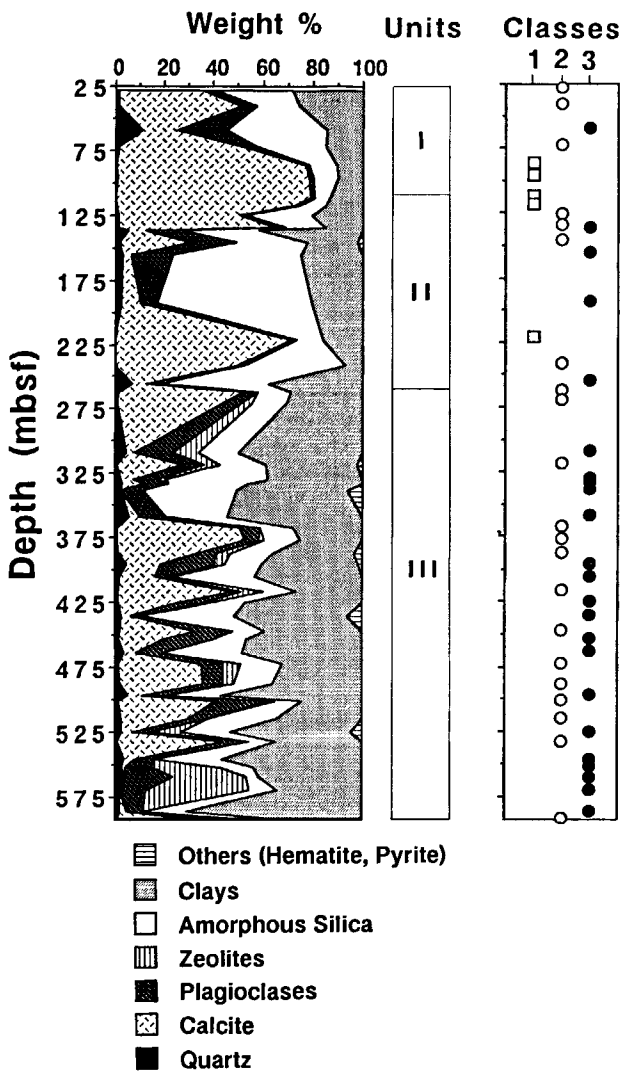

Figure 3

Halite-free mineral paragenesis and classes of sediments vs. *depth for Site 840.*

Paragenèses minérales (dessalées) et classes sédimentaires en fonction de la profondeur, Site 840.

Major element chemistry

Comparison between the amounts of the major solid phases and the concentrations of the chemical elements reveals three classes of sediment (Table 5), previously identified in Lau Basin sediments (Blanc, 1994):

Class 1 : biogenic calcite-rich sediments: 5 samples with 4 collected between 85 and 120 mbsf and one at 221.49 mbsf;

Class 2 : biogenic and volcanogenic mixed sediments : 21 samples;

Class 3 : volcanogenic material rich sediments: 23 samples, with 21 are below 135 mbsf.

The plots of CaO versus calcite (r = 0.97) (Fig. 4*a*) and SiO_2 versus amorphous silica + clays + feldspars (r = 0.94) (Fig. 4*b*) show that the Class 2 material appears to be intermediate between the two other classes, which approximate chemical end-members. Sediments from Class 1 are mainly characterized by their calcite content (73.4%) whereas sediments from Class 3 are mineralogically characterized by their abundance of silicate, mostly in the form of clays, amorphous silica and feldspars. The distribution of the three sedimentary classes with depth, (and consequently, with age) (Fig. 3) shows the temporal variation of the volcano-sedimentary production, and therefore, the temporal variation of the arc volcanism production. Volcanoclastic sediment and carbonate formation alternated during the major part of the late Miocene, whereas the volcanic input strongly decrease from 5.3 Ma to the Holocene.

The diagram of Fe_2O_3 + TiO_2 + MgO concentrations *versus* clays + zeolites content shows that the increase in Fe, Ti, and Mg is correlated with the amount increase of minerals resulting from the alteration of volcanic material, especially clays and zeolite minerals (Fig. 5). This alteration results principally in the replacement of the volcanic glass by smectite, but three samples from the bottom of the sedimentary column (840B-59X3 552.08 mbsf; 840B-60X1 560.08 mbsf; and 840B-61X2 570.13 mbsf) are enriched in zeolites, and contain 26.5%, 28.5%, and 41% of zeolite minerals respectively. These zeolite-rich sediments are distinct from the other volcaniclastic sediments by virtue of their strontium content (500 ppm for the zeolite-rich samples, against 200 ppm in average for the other Class 3 samples). The most important zeolite present in the zeolite-rich sediment corresponds to the Heulandite species. At Site 840, diagenetic processes appear from 250 mbsf to 550 mbsf, but remain limited. K_2O content averages 1% in the Class 3 samples rich in volcaniclastic material. These diagenetic processes are reflected by an increase in clay content with depth and the formation of small quantity of zeolite mineral (Fig. 3). Below 550 mbsf, the formation of abundant zeolite minerals give evidence of an increase of the diagenetic processes.

n° ODP	Depth (mbsf)	Inter I/S %	Smectite %	Chlorite %	Kaolinite %	Illite %
840C 3H2S	59.9	XXX		X	E	
840C 4H4S	72.5	XXXX		E		
840B 12X4	111.5	XXX		X		
840B 13X2S	118.1	XXXX				
840B 15XCC	134.42	XXX		X		
840B 24X1A	221.49	XXX		X		
840B 26X1	240.79	XXXX				
840B 28X2	262.21	XXXX				
840B 29X1	269.99	XXXX				
840B 33X1	308.64	XXX		X		
840B 34X1	318.45	XXXX				
840B 35X2	330.02	XXXX		E		
840B 39X2	359.01	XXX		X	E	
840B 41X1	376.41	XXX		X		
840B 42X2	387.04		XXXX			
840B 43X1	395.85		XXXX	E		
840B 46X1	424.72		XXXX			
840B 49X1	452.61	XXXX				
840B 50X1	463.06	XXXX		E		
840B 55X3	514.3	XXXX		E		
840B 56X4	525.15		XXXX			
840B 58X5	546.22		XXXX			
840B 60X1	560.08		XXXX	E		E
840B 61X2	570.13		XXXX			
840B 62X6	586.55	XXXX				
840B 63X3	592.11	XXXX		E		

E ⩽ 5 % 5 % < X ⩽ 15 % 15 % < XX ⩽ 50 % 50 % < XXX ⩽ 75%
75 % < XXXX ⩽ 90 % XXXXX > 90 %

Table 4

Distribution of the clays content of Site 840.

Distribution et nature des argiles du Site 840.

	Class 1 (Wt %)	Class 2 (Wt %)	Class 3 (Wt %)
	Biogenic calcite-rich sediments (n=5)	Biogenic-volcanogenic mixed sediments (n=21)	Volcanogenic-rich sediments (n=23)
Calcite	73.4 +/- 3.1	40 +/- 10.1	6.7 +/- 6
Am. Silica	9.3 +/- 1.9	18.5 +/- 7.8	26.7 +/- 13.3
Clays	12.5 +/- 2.5	26.9 +/- 8.3	41.4 +/- 11.7
SiO2	10.4 +/- 2.5	36.1 +/- 6.9	56.8 +/- 5.6
Al2O3	2.5 +/- 0.5	8.8 +/- 1.8	13 +/- 1
CaO	44.7 +/- 2.2	23.7 +/- 8.6	5.7 +/- 2.8
MgO	0.65 +/- 0.2	2.3 +/- 1.01	3.3 +/- 1.27
Fe2O3	1.6 +/- 0.68	5.1 +/- 1.42	8 +/- 2.23
Na2O	0.06 +/- 0.01	1.8 +/- 0.62	3.8 +/- 0.74
K2O	0.05 +/- 0.00	0.37 +/- 0.21	1.1 +/- 0.35
TiO2	0.14 +/- 0.04	0.48 +/- 0.1	0.75 +/- 0.2
MnO	0.12 +/- 0.08	0.26 +/- 0.1	0.15 +/- 0.02
P2O5	0.18 +/- 0.02	0.21 +/- 0.02	0.22 +/- 0.05
SrO	0.15 +/- 0.01	0.08 +/- 0.02	0.03 +/- 0.02
L.O.I.	38.7 +/- 1.3	20.7 +/- 7.6	7.05 +/- 2.3

Table 5

Average content of major mineral phases and average element concentrations of sediment from Class 1 (Biogenic calcite-rich sediment), Class 2 (Biogenic-volcanogenic mixed sediments), and Class 3 (Volcanogenic-rich sediments), Site 840.

Quantité moyenne des principaux minéraux et concentration moyenne des éléments majeurs des sediments des classes 1 (sédiments riches en calcite biogénique), 2 (mélange de sédiments volcaniques et de calcite biogénique), et 3 (sédiments riches en matériel volcanoclastique), Site 840.

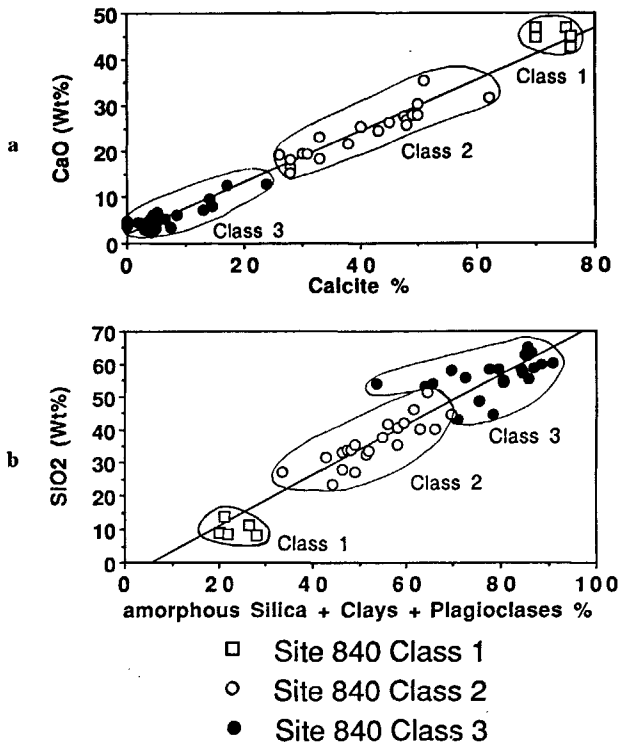

Figure 4

Concentration of CaO vs. *calcite content (a), concentration of SiO2 vs. amorphous silica + clays + plagioclase content (b), Site 840.*

Concentration en CaO en fonction des teneurs en calcite (a), concentration en SiO_2 en fonction des quantités de silice amorphe, d'argiles et de plagioclases (b) des sédiments du Site 840.

We have seen above the relationships between major element chemistry and the mineralogical phases. Some others elements, such as Rare Earth Elements, (REE) may be incorporated in specific mineralogical phase and we shall attempt to determine whether this appears in sediment from the Tonga Platform, through an investigation of the REE fractionation.

REE fractionation

Fractionation between the light and heavy REE may be expressed by the La/Yb ratio (Glasby *et al.*, 1987; Kunzendorf *et al.*, 1988, 1993). The La/Yb ratio is 4.54 +/- 2.1 and 2.54 +/- 1.5 for samples from Classes 2 and 3, respectively (Fig. 6); this is comparable with the La/Yb ratio of 1 to 8 found for Lau Basin sediment samples (Kunzendorf *et al.*, 1988). The La/Yb ratio reaches 15.1 +/- 2.6 for sediment samples from Class 1. Such high La/Yb ratios have been determined in foraminifera test from Atlantic Ocean sediments (Palmer, 1985), and in carbonate ooze from Pacific pelagic sediments (Toyoda *et al.*, 1990). The high La/Yb ratios of Site 840 samples derive from the strong depletion of Yb in the sediments enriched in calcium. Yb is the only REE analysed which correlates with the calcite content of the sediments (r = 0.833), whereas La, Ce and Lu do not show correlation with any mineral phase.

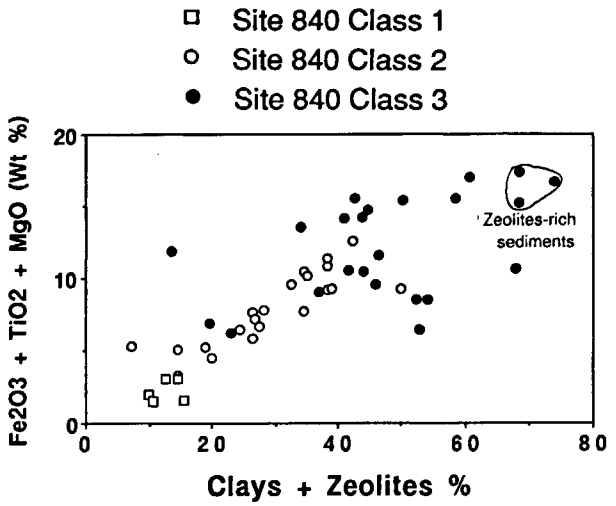

Figure 5

Concentration of Fe_2O_3 + TiO_2 + MgO vs. *clays and zeolite content, Site 840.*

Concentration en Fe_2O_3, TiO_2 et MgO en fonction des teneurs en argiles et zéolites, Site 840.

Volcanic rocks

Based on chemical data, together with mineralogical observation made on board, an origin of the volcanic rocks of the sedimentary column of Site 840, from the Tonga Platform could be proposed.

Sediments at Site 840 are characterized by a high volcaniclastic input from sediment gravity flows, mainly in the form of silty to sandy turbidites. Shipboard analyses of

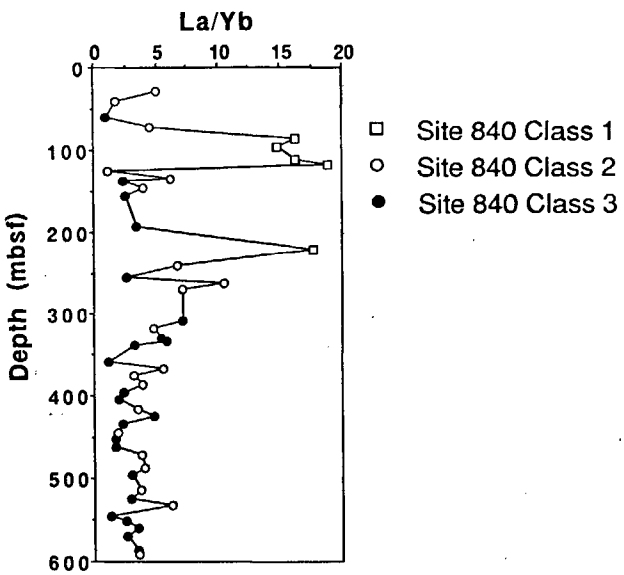

Figure 6

Distribution of La/Yb ratio vs. *depth, Site 840.*

Variation du rapport La/Yb en fonction de la profondeur, Site 840.

glass shards and laboratory X-ray diffraction and chemical analysis of the bulk rocks from the Tonga Platform showed that alteration of volcaniclastic sediment is limited, except in the zeolitic zone near the bottom of the hole. Volcanic glasses are basaltic to rhyodacitic in composition as estimated by their refractive indices and are dominated by intermediate composition (Parson, Hawkins, Allan *et al.*, 1992). Thus, we assume that for many elements, the bulk chemical composition of the volcanic sand and sandstone samples can be used as a rough estimate for the average composition of volcanic sources in a carbonate-free K_2O *vs.* SiO_2 diagram (Peccerillo and Taylor, 1976). In the diagram (Fig. 7), Class 2 and 3 samples from Site 840 lie in the fields of the low-K calc-alcaline and calc-alcaline series, and have the compositions of acid andesites, dacites and rhyolites.

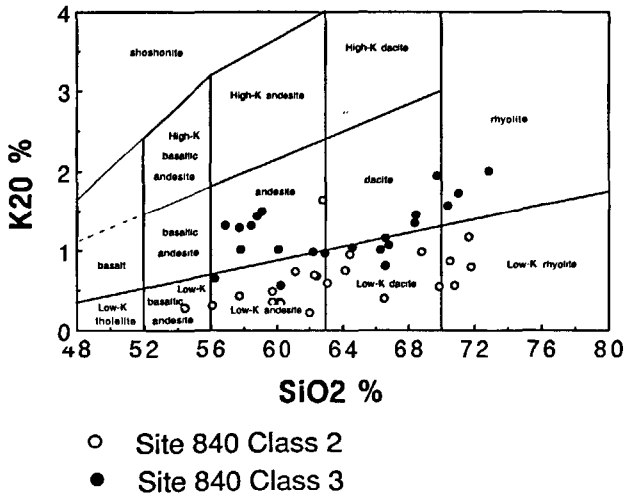

Figure 7

Carbonate-free K_2O vs SiO_2 content for Site 840 biogenic calcite and volcanogenic mixed sediments (C2) and volcanogenic material rich sediments (C3), Site 840 from the Tonga Platform.

Teneurs en K_2O en fonction de SiO_2 des échantillons décarbonatés des classes C2: mélange de sédiments volcaniques et de calcite biogénique et C3: sédiments riches en matériel volcanique du Site 840 de la plate-forme Tonga.

Interstitial water chemistry

Six interstitial water samples were collected from the upper part (60 to 150 mbsf) of the Site 840 drillhole (Table 6, Fig. 8). In the uppermost 300 mbsf, the low recovery and the coarser-grained sand nature of the sand-volcanic gravel lithologies limited the sampling. Below 300 mbsf, the relatively hard sediments were so well lithified that interstitial water could not be squeezed from them.

Interstitial water Cl and Na concentrations are fairly uniform and closely match those of average sea water concentrations (Broecker and Peng, 1982). Comparison with average sea water composition indicates an increase in Ca concentration and a decrease in Mg concentration in the uppermost 60 mbsf. These changes with depth are moderately high for deep-sea sediment interstitial waters (Lawrence and Gieskes, 1981; Gieskes and Lawrence, 1981) and probably reflect, therefore, the alteration of volcanogenic material in the sediments by incorporation of the magnesium in clay minerals and the calcium released in interstitial waters by the volcanogenic material. Below 70 mbsf, the Ca content in interstitial water no longer increases, perhaps due to a low precipitation of calcite below this depth. This is also suggested by the low alkalinity values determined in the most enriched carbonate layer (*e.g.* from 70 to 120 mbsf) (Table 6).

Concentrations of SO_4 and NH_4 do not vary to any great extent (Table 6), indicating that bacterial activity in these organic carbon-poor sediments is minimal. This is consistent with an alkalinity controlled by carbonate precipitation, and with the low level of dissolved manganese identified at Site 840. Below 120 mbsf, the slight increase in Mn suggests that the sub-bottom redox conditions were just sufficient to mobilize Mn.

The presence of dissolved SO_4, known to inhibit the dolomitization processes (Baker and Kastner, 1981) explains the absence of dolomite. This reinforces the interpretation that the Mg depletion is the result of removal during alteration of the volcanogenic materials.

The concentration-depth profile of K observed at Site 840 indicates that the decrease found for this element results from uptake by secondary minerals, predominantly smectite.

The concentration-depth profile of dissolved Sr shows an increase in Sr from standard sea water concentrations at the mud line to the interval 70-110 mbsf. Below Unit I, lower values are observed. Rapid increases in interstitial water

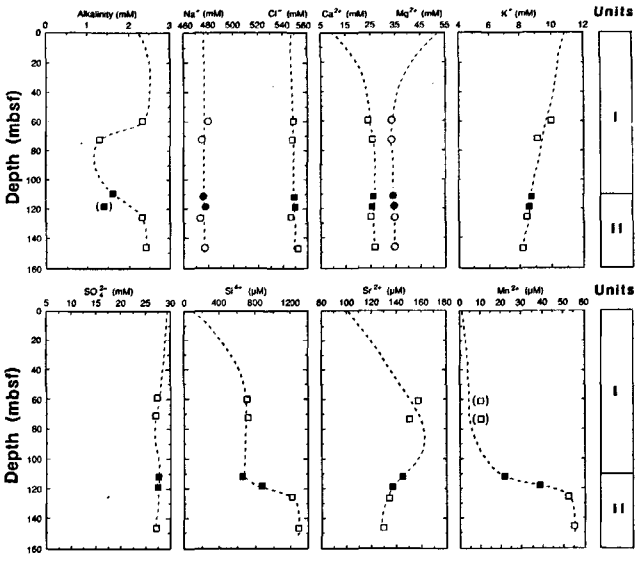

Figure 8

Concentration vs. depth profiles for alkalinity, sodium and chloride, calcium and magnesium, potassium, sulphate, silica, strontium, and manganese, Holes 840B and 840C. Filled symbols = samples from Hole 840B, and open symbols = samples from Hole 840C. Dashed lines begin at 0 mbsf at standard sea water concentrations.

Profils de concentration en fonction de la profondeur de l'alcalinité, du sodium et des chlorures, du calcium et du magnésium, du potassium, des sulfates, de la silice, du strontium et du manganèse des forages 840B et 840C. Symboles pleins: échantillons du puits 840B, symboles vides: échantillons du puits 840C. Les lignes en pointillés débutent à 0 mètre sous la surface du plancher océanique, aux concentrations de l'eau de mer.

n° ODP	Hole	Depth (mbsf)	pH	Alkalinity (mM/l)	Ca (mM/l)	Mg (mM/l)	K (mM/l)	Cl (mM/l)	SO_4 (mM/l)	NH_4 (µM/l)	Si (µM/l)	Sr (µM/l)	Mn (µM/l)	Na (mM/l)
3H2S	C	59.9	8.48	2.328	23.8	33.5	9.97	548	27.7	31	695	157	< 10	478
4H4S	C	72.5	7.42	1.279	25.4	33.3	9.08	547	26.9	73	709	150	< 10	474
12X4	B	111.5	7.43	1.745	25.8	33.8	8.76	549	27.7	36	647	145	21.5	475
13X2	B	118.1	7.35	1.418	25.6	34.3	8.57	550	27.5	42	866	136	38.9	477
5H1	C	125.5	7.69	2.296	24.8	34.7	8.44	546	27.3	29	1213	133	52.3	473
7H2	C	146	7.47	2.391	26.4	34.5	8.18	552	27.2	70	1295	128	54.8	476
Average Seawater			7.8	2.3	10.1	54.4	10.18	558.5	28.86	9	100	92.1	0	478.8

Table 6

Interstitial water chemistry data, pH, alkalinity, Ca, Mg, K, Cl, SO_4, NH_4, Si, Sr, Mn, Na, Site 840.

Valeurs du pH, de l'alcalinité et des concentrations en Ca, Mg, K, Cl, SO_4, NH_4, Si, Sr, Mn, et Na des eaux interstitielles du Site 840.

strontium concentration in carbonate sediments have usually been interpreted in terms of carbonate diagenesis (Sayles and Manheim, 1975; Gieskes, 1983; Baker, 1985; Chester, 1990). The decrease in dissolved Sr below the carbonate-rich sediments could result from the integration of Sr in zeolites, such as heulandite, increasingly present with depth.

Dissolved Si concentration probably increases from standard sea water values at the mudline to the first interstitial-water sample taken in lithologic Unit I. Silica concentration remains fairly constant at about 684 +/– 32 mM/l throughout Unit I. In Unit II, from 112 to 125 mbsf, a sharp increase in silica is observed, reaching 1213 mM/l at 125.5 mbsf. The Si concentration obtained from the deepest sample at 146 mbsf is slightly higher (1295 mM/l). This trend is probably related to the proportions of volcanogenic material in Units I and II.

Comparison with other sites from Leg 135

Classes of the Leg 135 sediments.

Sediments collected during Leg 135 provide an opportunity to compare the chemical and mineralogical variation in a back-arc basin (Lau Basin), and the trench margin of an active volcanic arc (Tofua Arc). Data required for this comparison are given by Blanc (1994) for Sites 834-839 from the Lau Basin and by Vitali *et al.* (1995) for Site 841 from the Tonga Trench Margin.

The sedimentary sequences recovered at Lau basin Sites 834-839 consist predominantly of a sequence of pelagic clayed nannofossil ooze containing interbeds of volcanic material which overlies a sequence dominated by redeposited volcanoclastics. The volcanoclastic units at Sites 836-839 are therefore much thicker and coarser-grained than at Sites 834-835. The maximum depth cored was 186.3 mbsf (Site 839). The basement ages range from 0.6 Ma (Site 836) to 4 Ma (Site 834).

Site 841 was drilled on the Tonga fore-arc, about 140 km south-southeast of Site 840. The sedimentary sequence at Site 841 consists of 605 m of clays, vitric siltstones, vitric sandstones, volcanic conglomerates and breccias, and calcareous volcanic sandstones. These sediments range in age from the middle Pleistocene to the late Eocene. Below 605 mbsf, drilling penetrated a rhyolitic volcanic complex (Parson, Hawkins, Allan *et al.*, 1992).

On the basis of the same criteria as for Site 840 from the Tonga Platform, sediments from Sites 834-839 from the Lau Basin present a similar distribution in three classes depending on their enrichment in biogenic calcite (Class 1) or in volcanogenic material (Class 3) and, with Class 2, material that appears to be intermediate between the two other classes (Fig. 9). A noticeable chemical difference is the occurrence of MnO in Class 1 and Class 2 from the Lau Basin (2.3% and 1.8% respectively). This concentration of manganese originates predominantly from the hydrothermal activity of the East Lau Spreading Centre and Central Lau Spreading Centre (Blanc, 1994). With respect to the major mineralogical variations between sites from the Lau Basin and from the Tonga Platform, zeolites are virtually absent in the three classes from the former, but the deepest sample analysed was situated only at 186.3 mbsf (Core 839A 21Xcc), whereas abundant zeolite zones have been described below 560 mbsf in Site 840 from the Tonga Platform.

Samples from Site 841 can also be separated into three classes, with Classes 2 and 3 similar to those of the Lau Basin and Tonga Platform, at least concerning the chemistry. The third class, named the Rhyolite Tuff Class (RTC) comprises rocks belonging to the rhyolitic volcanic complex cored below 605 mbsf. Whatever the class, samples from Site 841 show an enrichment in potassium resulting from active diagenetic processes occurring within the sediments (Vitali *et al.*, 1995). Alteration of the volcanogenic material, which constitutes the major part of the sedimentary column, is especially reflected at Site 841 by the very high proportion of zeolite minerals (17.8% and 25.3% for Classes 2 and 3, respectively). The Rhyolite Tuff Class yields chemical compositions similar to those of Class 3 from all the sites of Leg 135, but is characterized by its distinct mineralogical composition. Thus, the amount of quartz in this Rhyolitic Class accounts for about 30% of the whole rock. Clays (31%), plagioclases (19%) and amorphous silica (14%) constitute the other significant phases of the Rhyolitic Class, whereas zeolite minerals are absent.

The singularity of Site 841 sediments from the Tonga Trench Margin with respect to those from the Lau Basin and Tonga Platform sediments derives from the absence of Class 1 sediments, which are present in similar proportions in the Lau Basin and the Tonga Platform, and the occurrence of a Rhyolitic Tuff Class. The absence of carbonate-rich sediment results probably from two major factors: sedimentation below the Carbonate Compensation Depth

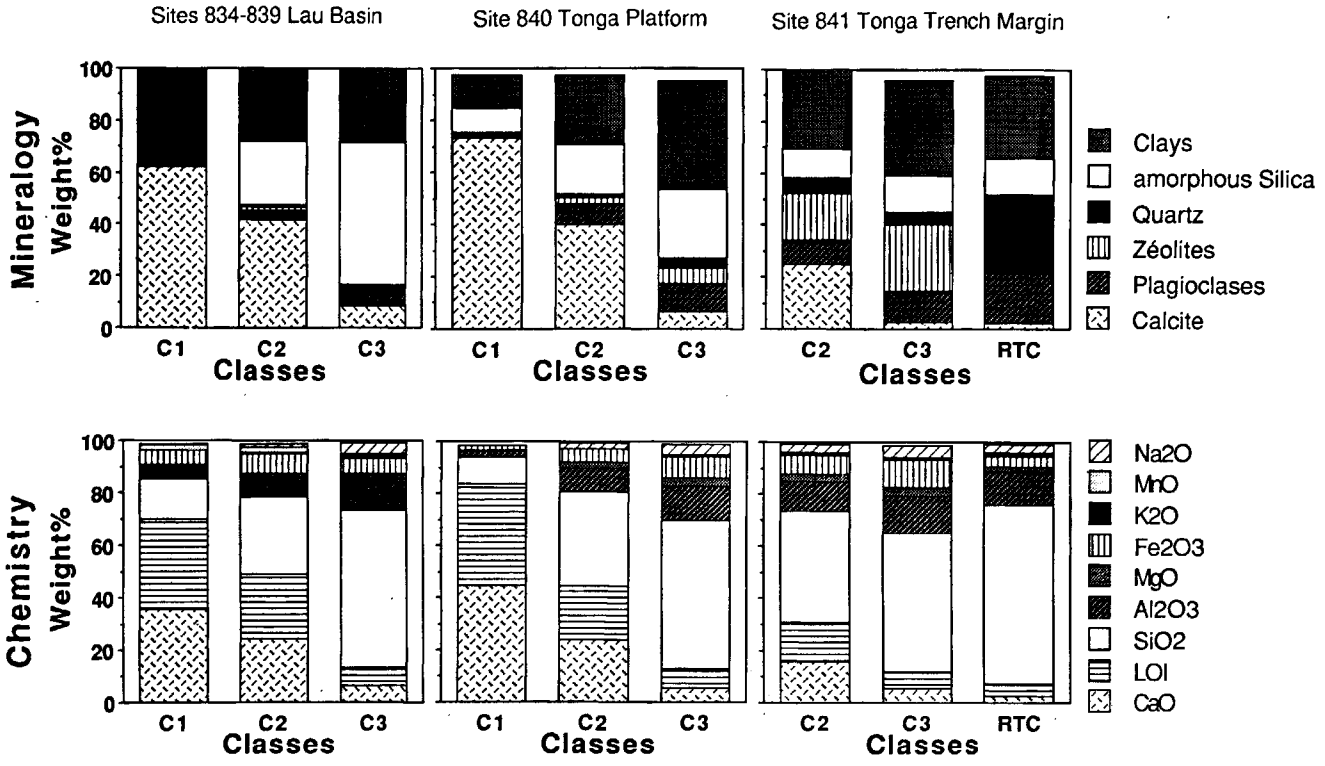

Figure 9

Chemistry and mineralogy of the classes of sediment from the Leg 135 Sites: Site 834-839 from the Lau Basin (Blanc, 1994), Site 840 from the Tonga Platform, and Site 841 from the Tonga Trench Margin (Vitali et al., *1995). C1: biogenic calcite rich sediments, C2: biogenic calcite and volcanogenic mixed sediments, C3: volcanogenic material rich sediments, RTC: Rhyolite Tuff Class.*

Chimie et minéralogie de chacune des classes de sédiments des Sites du Leg 135. L'échantillonage concerne les Sites 834-839 du bassin de Lau (Blanc, 1994), le Site 840 de la plate-forme Tonga, et le Site 841 de la bordure de la fosse Tonga (Vitali *et al.*, 1995). C1: sédiments riches en calcite biogénique, C2: mélange de sédiments volcaniques et de calcite biogénique, C3: sédiments riches en matériel volcanoclastique, RTC: classe des tufs rhyolitiques.

and diagenetic processes. At Site 841, deposits from Pleistocene to lower Pliocene occured below the CCD (Parson, Hawkins, Allan *et al.*, 1992), and assemblages from the upper Miocene, which constitute the major part of the sedimentary column, show varying degrees of dissolution resulting from deposition at or near the CCD, as well as diagenetic effects reflected by the high content of zeolite minerals.

The point underlined by this study is the very low abundance of manganese deposits at Site 840 and Site 841. The Tonga Ridge seems to constitute a barrier too high for the hydrothermal plumes from the Lau Basin to spread out. Comparison between Lau Basin and Tonga Platform minor and trace element concentrations will throw more light on the occurrence or absence of hydrothermal input from the Lau Spreading Centres.

Minor and trace element variations

In order to compare the minor and trace element concentration variations between Site 840 from the Tonga Platform and average carbonate deep sea marine sediments, and others sites from the Leg 135 sites, average analytical data from Class 1 of the Lau Basin and the Tonga Platform have been normalized to DSCRS (Deep-Sea Carbonate-Rich Sediments), defined by Turekian and Wedepohl (1961) as the carbonate-rich sediment end-member (Fig. 10). Tonga Platform Class 1 sediments show minor and trace element concentrations close to the DSCRS average concentration, whereas Class 1 sediments from the Lau Basin present higher values, especially in Mn.

Elements as V and Sc which are related to the clay fraction as previously observed (Kunzendorf *et al.*, 1990; Blanc, 1994) show higher concentrations in the Class 1 sediments from the Lau Basin than in the Class 1 sediments from the Tonga Platform. This is due to the higher clay fraction content in the Class 1 sediments from the Lau Basin than in the Class 1 sediments from the Tonga Platform.

Lau Basin sites show ore-forming element (Mn, Ba, Zn, Cu, Co, Ni, and Cr) concentrations which are much higher than from sites from the Tonga Platform. In addition, the amounts of P_2O_5 and Y in hydrothermal sediments from the Lau Basin (Blanc, 1994) are more than 5 times greater than in sediments from the Tonga Platform and from the Tonga Trench Margin. The difference in all these minor element concentrations between sites from the Lau Basin and the other sites of Leg 135 also indicates that hydrothermal input from the Lau Basin did not affect the chemical composition of the sediments of the Tonga Platform and Tonga Trench Margin, which suggests that the height of the Mn plume did not reach 1750 m above the sea floor of the Lau Basin. The higher Mn accumulation rates calculated in this back-arc basin, which attain values 40 times higher than those from the East Pacific Rise, can be best understood in terms of

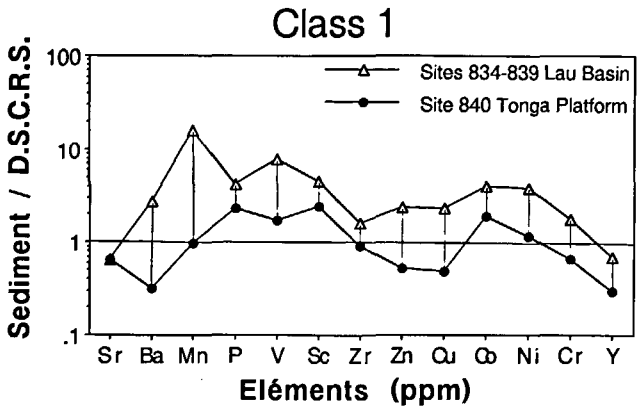

Figure 10

Lau Basin (Sites 834-839) and Tonga Platform (Site 840) average analysed minor and trace element concentrations from carbonate-rich sediments (Class 1), normalized to Deep-Sea Carbonate-Rich Sediments DSCRS, from Turekian and Wedepohl, 1961).

Concentrations moyennes des éléments mineurs et en traces du bassin de Lau (Sites 834-839) et du Site 840 de la plate-forme Tonga, normalisées aux sédiments marins profonds riches en carbonate (d'après Turékian et Wedepohl, 1961).

ponding sedimentation (Blanc, 1994), because all Mn produced by the hydrothermal activity was essentially accumulated in the limited area of the Lau Basin. Mn and elements such as Fe, Ti, and Al will be used to try to determine the sources of the sedimentary components from the Tonga Platform, the Lau Basin and the Tonga Trench Margin Sites.

Source components

The Site 840 Fe/Mn ratios are considerably greater than 3 for all units. This could be a preliminary argument for a terrigenous origin (Boström *et al.*, 1973; Bishoff *et al.*, 1979) of the Site 840 sediments from the Tonga Platform.

The ratio Al/(Al+Fe+Mn) is generally used as an index of detrital component, and a ratio greater than 0.4 is considered to indicate a detrital source in marine sediments (Boström and Peterson, 1969; Boström *et al.*, 1971; 1973). All studied samples from Site 840 show ratio values greater than 0.4. The multi-element plot is a method of visually partitioning source components in sedimentary rocks. A plot of Fe/Ti vs. Al/(Al+Fe+Mn) clarifies source components (Fig. 11). The Leg 135 samples show a trend between terrigenous and hydrothermal end-members with a slight displacement toward the oceanic crust end-member for the Lau Basin sediments, suggesting that submarine "MORB-like" oceanic crust could be a contributory source of sedimentary material for Lau Basin samples from Sites 834-839. The extension of the Lau Basin, which is < 5 m.y. old, is accompanied by intrusion of basalt assimilated to mid-ocean ridge tholeiite (Gill, 1976) that could explain the deviation toward the oceanic tholeiitic basalt end-member. The hydrothermal influence affecting Sites 834-839, situated on the western flanks of the Central Lau Spreading Centre and of the East Lau Spreading Centre, are clearly visible on the plot. Furthermore, the samples

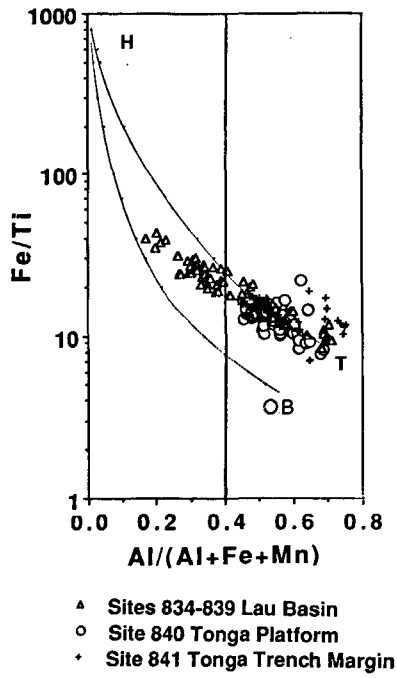

Figure 11

Plot of Fe/Ti vs. Al/(Al+Fe+Mn) for Sites 834-839 (Lau Basin) Site 840 (Tonga Platform) and Site 841 (Tonga Trench Margin) samples. (from Boström et al., *1973)*

H : Hydrothermal compositional end-member.
T : Terrigenous compositional end-member (sensus lato).
OB : Oceanic basalt compositional end-member (MORB).

Rapports Fe/Ti en fonction de Al/(Al+Fe+Mn) pour les échantillons des Sites 834-839 (bassin de Lau), Site 840 (plate-forme Tonga), et Site 841 (bordure de la fosse Tonga). (D'après Boström *et al.*, 1973)

H : Pôle hydrothermal.
T : Pôle Terrigène (*sensus lato*).
OB : Pôle Basalte océanique (MORB).

which plot closest to the hydrothermal end-member were collected from holes 834 and 835. This sustains the assumptions of a hydrothermal ponding fraction preferentially accumulated within the sediment of the northern part of the Lau Basin (Blanc, 1994).

The chemical data from Sites 840 and 841 fall wholly in the terrigenous field (*sensus lato*). This indicates firstly that submarine weathering of the oceanic crust has been a negligible source of sedimentary material for these sites and secondly that the hydrothermal influence of the Lau Basin Spreading Centres seems to be non-existent in the sediments from Site 840 of the Tonga Platform and Site 841 from the Tonga Trench Margin, despite the proximity of the active spreading centre, the Valu Fa ridge, which was postulated by Morton and Sleep (1985) as a southward extension of the East Lau Spreading Centre. The distribution of values from Site 840 and 841 samples near the terrigenous end-member (*sensus lato*) suggests some submarine more "arc-like" rocks, which correspond in this area to the "emerged volcanic material" from the Tofua active arc.

The plot of Fe/Ti *vs.* Al/(Al+Fe+Mn) shows that hydrothermal activity and alteration of the oceanic crust may

influence the composition of the Lau Basin sediments deposits; therefore South West Pacific volcanic activity represents the main contributor to the non-biogenic carbonate sediments found at all sites from Leg 135, as previously reported (Parson, Hawkin, Allan *et al.*, 1992). In the following, the average composition of these volcanic rocks from Leg 135 is estimated from a K_2O *vs.* SiO_2 diagram.

Leg 135 volcanic rocks

Data from all the sites of Leg 135, *e.g.* Sites 834-839 from the Lau Basin (Blanc, 1994), Site 840 from the Tonga Platform, and Site 841 from the Tonga Trench Margin (Vitali *et al.*, 1995) have been plotted on the carbonate-free K_2O *vs.* SiO_2 diagram (Figure 12). In order to restrict the error made on K_2O and SiO_2 recalculated values on a carbonate-free basis, we have used for the comparison only sediments rich in volcaniclastic material (Class 3) from all the sites, and the Rhyolitic Tuff Class from Site 841.

The shipboard analyses of glass shards from the Sites 834-839 Lau Basin sediments lead to the conclusion that alteration was limited at these sites. Values of SiO_2 and K_2O of the Lau Basin volcaniclastic sediment show distributions similar to those of the Tonga Platform, suggesting composition ranging from andesitic to dacitic and even rhyolite, as previously mentioned for superficial sediments (von Stackelberg *et al.*, 1988; Frenzel *et al.*, 1990).

Chemical and mineralogical studies from Site 841 have shown the importance of diagenetic process at this site mainly composed by Miocene volcano-sedimentary deposits (Vitali *et al.*, 1995). Diagenesis is reflected by an increase in the K_2O content, as seen in the K_2O-SiO_2 plot. Potassium is known to be particularly mobile both during weathering and later burial of volcanic material (Nesbitt and Young, 1982; 1989). All the samples from Site 841 that plotted on the rhyolite part of the diagram belong to the undated Rhyolite Tuffs Class that forms the lower part of Hole 841B from the Tonga Trench Margin (Parson, Hawkins, Allan *et al.*, 1992). High-silica rocks have been previously found in the Tonga Trench Slope (Vallier *et al.*, 1985), and in the Mariana frontal Arc (Meijer, 1983). These high SiO_2 volcanic rocks are unusual for intra oceanic island arcs and their origins are the subject of debate.

Rhyolite glasses in the Lau Basin, Tonga Platform and Tonga Trench Margin probably result from a low-K material before the alteration processes. The occurrence of rhyolite glasses in these three areas raises the question of their origin. Do the rhyolitic glasses belong to the siliceous end-member of a low-K andesite series, or do they derive from an independant phenomenon ? If all the rhyolitic material from Leg 135 is genetically linked, the age of the rhyolitic complex discovered under the Tonga Trench could be estimated. Indeed, dated rhyolitic glass samples at Sites 834-839 from the Lau Basin and at Site 840 from the Tonga Platform are younger than 2 Ma and 6.5 Ma respectively (Parson, Hawkins, Allan *et al.*, 1992). However, this hypothesis requires substantiation from chemical and isotopic studies of the pure fraction of rhyolitic vitric shards from all the sites. Altenatively, the rhyolite complex cored at Site 841 could have originated in the tectonic erosion of the active margin, leading to a seaward displacement of the 17-34 Ma fore-arc (Lallemand, 1992). In this case, the nature of the volcanic product was changed since the eocene period.

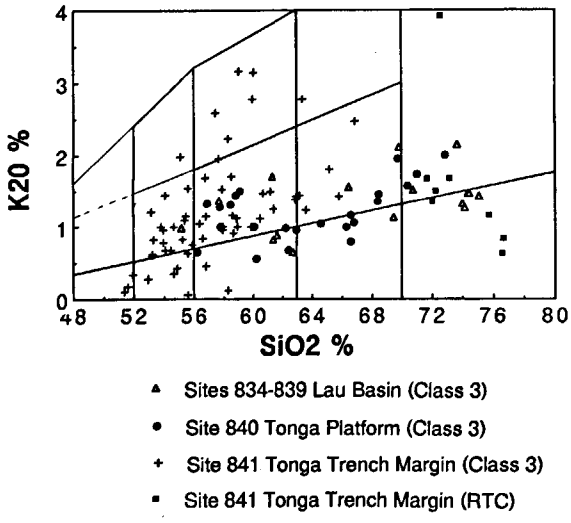

Figure 12

Carbonate-free K_2O vs. SiO_2 content for Leg 135 volcanogenic material rich sediments (C3), and for Site 841 Rhyolitic Tuff Class sediments.

Teneurs en K_2O en fonction de SiO_2 des échantillons décarbonatés de la Classe 3 (C3), sédiments riches en matériel volcanique du Leg 135, et des sédiments de la classe de Tufs Rhyolitiques (RTC) du Site 841 de la bordure de la fosse Tonga.

SUMMARY AND CONCLUSIONS

Three classes can be easily identified from the solid phases and the major chemical composition of samples from the Tonga Platform sediments: biogenic calcite-rich sediments (Class 1); biogenic calcite and volcanogenic mixed sediments (Class 2); and volcanogenic rich sediments (Class 3). The distribution of the three sedimentary classes with depth (and thus with age) reflects the temporal variation of the volcano-sedimentary production, and therefore, the temporal variation of the arc volcanism production. At Site 840, volcanoclastic sediment and carbonate formation alternated during the major part of the late Miocene, whereas the volcanic input strongly decreases from 5.3 Ma to the Holocene.

Alteration has resulted principally in the replacement of volcanic glass by smectite. Diagenesis is more accentuated at the bottom of the sedimentary column, as indicated by the abundance of zeolite minerals (heulandite, erionite, analcime and clinoptilolite). At Site 840, it would appear that alteration of volcanic material in the sediments is the major factor responsible for observed changes in the Ca, Mg, and K gradients in the interstitial waters. Concentrations of SO_4 and NH_4 do not greatly vary, indicating that bacterial activity in these low organic-carbon sediments is minimal. This is further substantiated by the low level of dissolved Mn. Between 70 and 110 mbsf, the observed decrease in alkalinity is probably caused by the precipitation of calcium

carbonate in response to an increase in Ca released in interstitial waters by the alteration of volcaniclastic material.

Unlike sediments from neighbouring Sites 834-839 from the Lau Basin that show similar chemical and mineralogical compositions, sediments of Site 840 from the Tonga Platform and also sediments of Site 841 from the Tonga Trench Margin do not show hydrothermal influence from the proximal Lau Spreading Centres. The Tonga Ridge seems to constitute a barrier too high for the hydrothermal plumes from the Lau Basin to spread out, and the non-carbonate fraction of Sites 840 and 841 results from the high input of andesitic to rhyolitic rocks from the volcanoes of this part of the SW Pacific.

Acknowledgments

The authors wish to thank two anonymous reviewers for their helpful comments and INSU-CNRS Geoscience Marine Committee for their financial supports.

REFERENCES

Baker P.A. (1985). Pore-water chemistry of carbonate-rich sediments, Lord Howe Rise, Southwest Pacific Ocean. *Initial Report of the Deep-Sea Drilling Project.* Vol. **90**, 1249-1256. Washington (U.S Govt. Printing office).

Baker P.A., and M. Kastner (1981). Constraints on the formation of sedimentary dolomite. *Science.* Vol. **213**, 215-216.

Blanc G. (1994). Geochemical Studies on selected sediment samples from the back-arc Lau basin, Leg 135 ODP. *Proceeding of the Ocean Drilling Program, Scientific Results.* Vol. **135**, 689-707.

Bishoff J.L., G.R. Heath and M. Leinen (1979). Geochemistry of deep sea sediments from the Pacific Manganese nodule province: Domes Sites A, B, C. in Bishoff J.L. and Piper D.Z. (Eds.). *Marine Geology and Oceanography of the Pacific Manganese Nodule Province. New York* (Plenum). 397-436.

Boström K. and M.N.A. Peterson (1969). The origin of aluminium-poor ferromanganoan sediments in areas of high heat flow on the East Pacific Rise. *Marine Geology.* Vol. **7**, 427-447.

Boström K., O. Joensu, S. Valdés and M. Riera (1971). Geochemical history of South Atlantic Ocean sediments since late cretaceous. *Marine Geology.* Vol. **12**, 85-121.

Boström K., T. Kraemerk and S. Gartner (1973). Provenance and accumulation rates of opaline Silica, Al, Ti, Fe, Mn, Cu, Ni, and Co in Pacific Pelagic sediments. *Chemical Geology.* Vol. **11**, 123-148.

Broecker W.S. and T.H. Peng (1982). *Tracers in the Sea.* Palisades, NY (Eldigo Press).

Chester R. (1990). Marine Geochemistry. *Unwin Hyman.* London, 698 p.

Cronan D.S., S.A. Moorby, G.P. Glasby, K. Knedler, J. Thomson and R. Hodkinson (1984). Hydrothermal and volcaniclastic sedimentation on the Tonga-Kermadec Ridge and in its adjacent marginal basins. *Geological Society of London.* Special publication **16**, 137-149.

Cronan D.S., R. Hodkinson, D.D. Harkness, S.A. Moorby, and G.P. Glasby (1986). Accumulation Rates of Hydrothermal Metalliferous Sediments in the Lau Basin. *Geo-Marine Letters.* Vol. **6**, 51-56.

Fouquet Y., J-L. Charlou, J-P. Donval, J-P. Foucher, F. Harmegnies, H. Pelle, U. von Stackelberg, M. Wiedicke, J. Erzinger, P. Herzig, H. Mühe, S. Soakai, and H. Whitechurch (1990). Hydrothermal activity in the Lau basin: First results from the Nautilau cruise. *EOS (Transactions, American Geophysical Union).* Vol. **71**, 18, 678-679.

Fouquet Y., U. von Stackelberg, J-L. Charlou, J-P. Donval, J-P. Foucher, J. Erzinger, P. Herzig, H. Mühe, M. Wiedicke, S. Soakai, and H. Whitechurch (1991). Hydrothermal activity in the Lau basin: Sulfides and water chemistry. *Geology.* Vol. **19**, 303-306.

Frenzel G., R. Mühe, and P. Stoffers (1990). Petrology of the volcanic rocks from the Lau Basin, Southwest Pacific. *Geol. Jb.* D **92**, 395-479; Hannover.

Gieskes J.M. (1973). Interstitial water studies, Leg 15, alkalinity, pH, Mg, Ca, Si, PO_4, and NH_4. *Initial Report of the Deep Sea Drilling Project.* Vol. **20**, 813-829. Washington (U.S Govt. Printing office).

Gieskes J.M. (1983). The chemistry of Interstitial Waters of Deep Sea Sediments: Interpretation of Deep Sea Drilling Data. *In* Riley J.P., Chester R. (Eds.), *Chemical Oceanography. London Academic Press.* Vol. **8**, 221-269.

Gieskes J.M., and J.R. Lawrence (1981). Alteration of volcanic matter in deep sea sediment: Evidence from the chemical composition of interstitial water from deep sea drilling cores. *Geochimica Cosmochimica Acta.* Vol. **45**, 1687-1703.

Gieskes J.M., and G. Petertsman (1986). Water chemistry procedures aboard *JOIDES Resolution* - some comments. *ODP Tech.* Note n°5.

Gill J.B. (1976). Composition and age of Lau Basin and Ridge volcanic rocks: Implications for evolution of an interarc basin and remnant arc. *Geological Society of America Bulletin.* Vol. **87**, 1384-1395.

Glasby G.P., R. Gwozdz, H. Kunzendorf, G. Friedrich and T. Thijssen (1987). The distribution of rare earth and minor elements in manganese nodules and sediments from the equatorial and S.W. Pacific. *Lithos.* Vol. **20**, 97-113.

Hodkinson R., D.S. Cronan, G.P. Glasby, and S.A. Moorby (1986). Geochemistry of marine sediments from the Lau Basin, Havre Through, and Tonga-Kermadec Ridge. *New Zealand Journal of Geology and Geophysics.* Vol. **29**, 335-344.

Hooton D.H. and N.E. Giorgetta (1977). Quantitative X-Ray Diffraction Analysis by a Direct Calculation Method. *X-Ray Spectrometry.* Vol. **6**, 1, 2-5.

Kunzendorf H., P. Stoffers, and R. Gwozdz (1988). Regional variations of REE patterns in sediments from active plate boundaries. *Marine Geology.* Vol. **84**, 191-199.

Kunzendorf H., P. Walter, P. Stoffers, and R. Gwozdz (1990). Rare and precious element geochemistry of sediments from the Lau Basin. *Geol. Jb.* D **92**, 263-278; Hannover.

Kunzendorf H., G.P. Glasby, P. Stoffers, and W.L. Plüger (1993). The distribution of rare earth and minor elements in manganese nodules, micronodules and sediments along an east-west transect in the southern Pacific. *Lithos.* Vol. **30**, 45-56.

Lallemand S. (1992). Transfert de matière en zone de subduction. *Mém. Sc. Terre. Université Pierre et Marie Curie.* n° 92/27. 295 p.

Lawrence J.R., and J.M. Gieskes (1981). Constraints on water transport and alteration in the oceanic crust from the isotopic composition of pore water. *J. Geophys. Res.* Vol. **86**, 7924-7934.

Manheim F.T., and F.L. Sayles (1974). Composition and origin of the interstitial waters of marine sediments based on deep sea drill cores. *In* Goldberg E.D (Eds). The Sea. **5**, 527-568.

Meijer A. (1983). The origin of Low-K Rhyolites from the Mariana Frontal Arc. *Contrib. Mineral Petrol.* Vol. **83**, 45-51.

Moorby S.A., K.E. Knedler, G.P. Glasby, R. Hodkinson and D.S. Cronan (1986). Lithology, colour, mineralogy, and geochemistry of marine sediments from the Lau Basin, Havre Through and Tonga-Kermadec Ridge. *New Zealand Oceanographic Institute. Oceanographic field report* **27**, 34 p.

Morton J.L., and N.H. Sleep (1985). Seismic reflections from a Lau Basin magma chamber. *In* Scholl D.W. and Vallier T.L. (eds): Geology and offshore resources of Pacific island arcs Tonga regions. *Earth Sciences Series.* Vol. **2**, 441-453.

Nesbitt H.W. and G.M. Young (1982). Early Proterozoic climates and plate motions inferred from major element chemistry of lutites. *Nature*, Vol. **299**, 715-717.

Nesbitt H.W. and G.M. Young (1989). Formation and diagenesis of weathering profiles. *The journal of Geology.* Vol. **97**, 129-147.

Palmer M.R. (1985). Rare earth elements in foraminifera tests. *Earth and Planetary Science Letters.* Vol. **73**, 285-298.

Parson L., J. Hawkins, J. Allan and Shipboard Scientific Party (1992). *Proceeding of the Ocean Drilling Program, initial report.* Vol. **135**. College Station, TX (Ocean Drilling Program).

Peccerillo A. and S.R. Taylor (1976). Geochemistry of Eocene Calc-Alkaline Volcanic Rocks from the Kastamonu Area, Northern Turkey. *Contrib. Mineral Petrol.* Vol. **58**, 63-81.

Samuel J., R. Rouault and Y. Besnus (1985). Analyse multi-élémentaire standardisée des matériaux géologiques en spectrométrie d'émission par plasma à couplage inductif. *Analusis.* Vol. **13** , 312-317.

Sayles F.L. and F.T. Manheim (1975). Interstitial solutions and diagenesis in deeply buried marine sediments: results from the Deep Sea Drilling Project. *Geochimica Cosmochimica Acta.* Vol. **39**, 103-127.

Toyoda K., Y. Nakamura and A. Masuda (1990). Rare earth elements of Pacific pelagic sediments. *Geochimica Cosmochimica Acta.* Vol. **54**, 4, 1093-1103.

Turekian K.K. and K.H. Wedepohl (1961). Distribution of the elements in some major units of the Earth's crust. *Bull. Geol. Soc. Amer.* Vol. **72**, 175-192.

Vallier T.L., R.M. O'Connor, D.W. Scholl, A.J. Stevenson and P.J. Quinterno (1985). Petrology of rocks dredged from the landward slope of the Tonga Trench: Implications for middle miocene volcanism and subsidence of the Tonga Ridge. *In* Scholl D.W and Vallier T.L., Geology and offshore resources of Pacific island arcs-Tonga region. *Circum-Pacific Council for Energy and Mineral Resources, Earth Science Series.* Vol. **2**, 109-120.

Vitali F., G. Blanc and Ph. Larqué (1995). Zeolite distribution in volcaniclastic deep-sea sediments from the Tonga Trench Margin (S.W. Pacific). *Clays and Clay Minerals.* Vol. **43**, 92-104.

von Stackelberg U., M. Gastner, G.P. Glasby, H. Gundlach, K. Johnson, O. Lettau, J. Lum, V. Marchig, J.L. Morton, W. Pohl, U. von Rad, V. Riech, W. Schmitz, P. Stoffers and M. Wiedicke (1985). Hydrothermal sulfide deposits in Back-Arc Spreading Centres in the Southwest Pacific. *Bundesanstalt für Geowissenschaften und Rohstoffe.* Circular 2.

von Stackelberg U., Y. Fouquet, R.D. Hansen, S. Helu, V. Marchig, J. Morton, W. Pohl, U. von Rad, H. Rask, V. Riech, B. Schlenker, S. Soakai, G. Sunkel, A. Stevenson, W. Weiss and T. Wichmann (1988) : Active hydrothermalism in the Lau Back-Arc Basin (SW-Pacific). First results from the SONNE 48 Cruise (1987). *Marine Mining.* Vol. **7**, 431-442.

von Stackelberg U., U. von Rad, V. Marchig, P. Muller and Th. Weiser (1990). Hydrothermal mineralization in the Lau and North Fiji Basins. *Geol. Jb.* D **92**, 547-613; Hannover.